Effects of Boundary Damping on Natural Frequencies in Bending Vibrations of Intelligent Vibrissa Tactile Systems

Carsten Behn
Christoph Will

Department of Technical Mechanics
Ilmenau Universiy of Technology, Germany
Email: carsten.behn@tu-ilmenau.de
christoph.will@tu-ilmenau.de

Joachim Steigenberger

Institute of Mathematics
Ilmenau Universiy of Technology, Germany
Email: joachim.steigenberger@tu-ilmenau.de

***Abstract*—This paper is devoted to the analytical investigations of transversal vibrations of beams, which exhibit discrete, viscoelastic, rotational and translational supports. The special structure of the beam models is caused by the consideration of animal vibrissae. Vibrissae are tactile hairs (of a tactile sense organ), which complement the audible and visual sense. There exist different types of these tactile hairs, where we do not want to distinguish the various types, because the tenor of our investigations is from biomimetics and bionics. Rather, we are interested in the special design of a vibrissa from the mechanical point of view. In contrast to many works from literature, which focus on (quasi-) static bending investigations, we try to investigate and to determine the effects of the special design of a vibrissa (e.g., viscoelastic supports due to the follicle sine complex and due to the skin) on the dynamic behavior, especially on the spectrum of (natural) frequencies. The knowledge of dynamical characteristics is important for the design of artificial sensors. We present various beams with different supports (clamped and pivoted with discrete viscoelastic couplings), which are to model the biological tissues. This is new in literature and is different from existing researches. We focus on investigations of the natural frequency spectra of various systems. A close examination of vibrissa-like beam models with boundary damping exhibits features that are unlike in comparison to classical vibration systems.**

Keywords–Bending beam vibrations; boundary damping; natural frequency; bio-inspired sensor; vibrissa.

I. Introduction & Motivation

This paper contributes to the development of intelligent tactile sensors and extends the results in the INTELLI 2014 paper [1]. There is a great interest in tactile sensors, since they have advantages in contrast to other sensor types. They are superior to optical sensors as in noisy environments (e.g., dark, murky water or in smoky air), and also cheaper in manufacture and use.

In the technical development, engineers often use biological systems as an inspiration. A tactile sensor system, which attracted attention in recent years, is the *animal vibrissa* found on, e.g., rats and mice. These hair-like sensors serve for the exploration of the environment, the animals use them, e.g., to detect outer objects, to distinguish between different surfaces, or to recognize surface textures, respectively.

For the functional understanding and analytical investigations, there are already various mechanical models for a vibrissa to explain the technical acquisition of information. In contrast to various works from literature [2] [3] [4] [5] [6], we focus on investigations of the vibrissa dynamics in this paper. For this, we utilize the *classical Euler-Bernoulli beam*, which is often used to analyze systems in technical disciplines like automotive engineering (e.g., power train vibration) and microsystems technologies (e.g., cantilever vibration). In recent years, this classical model is used to model and to understand effects of vibrissa sensor systems in biomechanics [7]. This is also the background of the work presented in the paper. Due to the biological paragon, we set up various mechanical models and analyze them in an analytical and numerical way.

The scope of the present paper is to contribute to the mechanical modeling of a technical vibrissa as tactile sensors for the distance detection. In later application of object localization and distance detection, we try to determine the natural frequency spectrum due to an obstacle contact (modeled as a sudden bearing to the beam, hence, sudden change of boundary conditions) and its shift (compared to the scenario of no contact) to calculate the distance of the obstacle to the base of the artificial vibrissa, see also [8] and [9].

But, in contrast to literature, we incorporate spring and damping elements as in [1], representing the biological tissue of animal skin and support of the vibrissa. This is rarely done in literature. Hence, we extend the results in [10].

For this, we start an introduction to the biological paragon, describing its functionality, presenting the state of art in modeling of hair-like sensor systems, and introduce the analytical treatment of transverse vibrations of beams due to [11] in the following and present the investigations of various vibrissa models.

II. The Paragon From Biology: Vibrissae

A paragon of (biological and artificial) tactile sensor systems is the animal vibrissae. Vibrissae are tactile hairs, can be found on, e.g., mice and rats, and complement the audible and visual sense. Mice and rats use their vibrissae (in the mystacial pad) to acquire information about their surroundings. The vibrissa itself (made of dead material) is mainly used as a lever for the force transmission. But, in contrast to ordinary hairs, vibrissae are stiffer and have a (assumed hollow) conical shape [12]. The mystacial vibrissae are arranged in an array of columns and rows around the snout, see Figure 1.

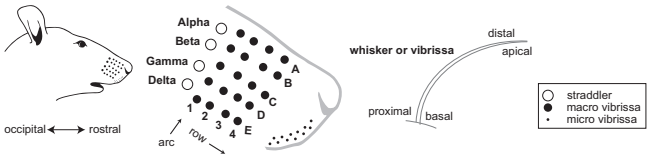

Figure 1. Schematic drawing of the mystacial pad, [12].

Each vibrissa is embedded in and supported by its own follicle-sinus complex (FSC). The FSC is characterized by its exceptional arrangement of blood vessels, neural connections and muscles. It is presumed that the rodents can control the viscoelastic properties of the vibrissa's support by regulating the blood supply to the sinus (like a blood sac) [13]. The functionality of these vibrissae vary from animal to animal and is best developed in rodents, especially in mice and rats [14]. The detection of contact forces is made possible by the pressure-sensitive mechanoreceptors in the support of the vibrissa (i.e., FSC). These mechanoreceptors are stimulated due to the vibrissa displacements in the FSC. The nerves transmit the information through several processing units to the Central Nervous System (CNS). The receptor cells offer the fundamental principle 'adaptation' [15] [16] [17] [18]. The muscle-system, see Figure 2 (adapted from [13] [19] [20] [21]) enables the rodents to use their vibrissae in two different ways (modes of operation):

- In the *passive mode*, the vibrissae are being deflected by external forces (e.g., wind). They return to their rest position passively — thus without any muscle activation, just via the fibrous band.
- In the *active mode*, the vibrissae are swung back- and forward by alternate contractions of the intrinsic and extrinsic muscles (with different frequencies and amplitudes). By adjusting the frequency and amplitude of the oscillations, the rodents are able to investigate object surfaces and shapes amazingly fast and with high precision [22].

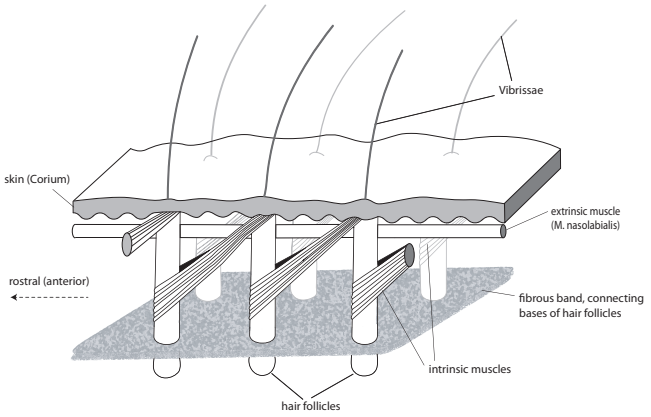

Figure 2. Schematic drawing of neighboring mystacial follicles [16].

Therefore, this biological sensor system is highly interesting for applications in the field of autonomous robotics, since tactile sensors can offer reliable information, where conventional sensors fail.

But, how the animals convert these multiple contacts with single objects into coherent information about their surroundings is still unclear. And it is not of main interest from our point of view: the tenor of our investigations is from bionics. The main focus is not on "copying" the solution from biology/animality, rather on detecting the main features, functionality and algorithms of the considered biological systems to implement them in (here: mechanical) models and to develop ideas for prototypes. We have to proceed in several steps, where step 1 to step 4 are usually of iterative manner, [18]:

1. analyzing live biological systems, e.g., here tactile hair system,
2. quantifying the mechanical and environmental behavior: identifying and quantifying mechanosensitive responses (e.g., pressure, vibrations) and their mechanisms as adaptation,
3. modeling live paradigms with those basic features developed before,
4. exploiting corresponding mathematical models in order to understand details of internal processes and,
5. coming to artificial prototypes (e.g., sensors in robotics), which exhibit features of the real paradigms.

Therefore, we present the state of art in modeling such sensor systems in the following.

Starting point and motivation of the following investigations are multiple **hypotheses** concerning the **functionality of the vibrissa**:

- The elasticity and the conical shape of the hair are relevant for the functionality of the vibrissa [2].
- The viscoelastic properties of the support (see the FSC) are controlled by the blood pressure in the blood sinus [13] [23].
- The vibrissae are excited with or close to their resonance frequencies during the active mode [24] [25].

Following these hypotheses, the primary tasks now are:

- to investigate the influence of elasticity and conical shape on the vibration characteristics of the vibrissa by analyzing its natural frequency spectrum;
- to analytically examine innovative models of a flexible vibrissa with a viscoelastic support, which fit the real object and its support better than models in literature.

III. State Of Art In Modeling Hair-like Sensors

An intensive literature overview of technical vibrissa models has been given in [16].

In the majority of papers found in literature, the development of innovative technical whiskers was poorly based on mechanical models of the vibrissa. In order to analyze the mechanical and especially the dynamical behavior of the vibrissa, the physical principles of the paradigm have to be identified. Therefore, abstract technical models, which describe the biological example in detail and are suitable to be analyzed using engineering and scientific methods, are sought.

Usually, two types of models are used to analyze the mechanical behavior of the vibrissa:

- *Rigid body models* form the vibrissa as a stiff, inelastic body. Such models have the advantage of a simple mathematical description and solution. Furthermore, these models can easily be used to analyze the influence of varying viscoelastic supports. However, neglecting the inherent elasticity of the vibrissa implies a questionable oversimplification of the biological example.
- *Continuum models* are closer to the biological paradigm, as the tactile hair is implemented as an elastic beam. They are thus able to take the inherent dynamical behavior and the bending stiffness of the biological vibrissa into account.

Some approaches to the modeling of the biological paragon vibrissa use rigid body models, in which a rod-like vibrissa is supported by a combination of spring and damping elements modeling the viscoelastic properties of the follicle-sinus complex. However, all the rigid body models can only offer limited information about the functionality of the biological sensory system. Therefore, we focus on continuum models and deal with bending problems of continuous beam systems. In the following, we summarize the relevant models of [16] without any valuation:

- Birdwell et al. analyzed the bending behavior in [2]. They set up a simple model, which is analyzed in a linearly way, i.e., the investigations are only valid for small deflections. An important feature therein was the incorporation of the conical shape to the bending behavior. They stated that this fact from biology is not negligible. Moreover, they found out that the Young's modulus of natural vibrissae varies, but they were still neglecting the support's compliance. Further on, they determined the clamping torques for a vibrissa model, which is only valid for small deflection. In this context, they found out that influence of the natural pre-curvature of the vibrissa is negligible, which is rather obvious from the mechanical point of view.
- Scholz and Rahn set up a model for profile sensing with an actuated vibrissa in [26]. They realized an active mode of a vibrissa, scanned various obstacle contours and reconstructed the shape in the following way: the one-sided clamped vibrissa was moved along an object, the clamping reaction were measured and then used for a numerical integration method the determine the shape of the deflected vibrissae, which form a envelope of the object. These results were improved from, first, a fully analytical way in [5] and then, secondly, in [6] were the authors present a reconstruction algorithm, which uses noise corrupted measurement data to reconstruct the object shape. A test rig for a experimental verification is presented in [26] and [27]. All these works focussed a one-sided clamped technical vibrissa where the support's compliance is also neglected.
- The groups of Neimark et al. [24] and Andermann et al. [25] set up a model for the determination of the support's influence on the resonance properties of natural vibrissae. The present experimental measurements of vibrissae's resonance frequencies (with dubious results during numerical evaluations, because a constant Young's modulus is used for all vibrissae. Their finding was a massive influence of the support on the resonance frequencies. Furthermore, they determined only of the first frequencies of the vibrissae. Analyzing the transduction and processing of the frequency provoked stimuli to the CNS, hence the resonance frequencies contain relevant information.

Most of the models in literature, in particular the rigid body models, are just results of anatomic investigations. They do not directly aim at bionic applications. Further on, some models are very exact, but too complex to gain deeper insight the system to identify the essential mechanical elements.

On the other hand, in particular, concerning continuum beam models, the level of mathematical investigations is rather low:

- linear bending theory with very simple conclusions,
- mixing of linear and nonlinear theories, and
- using boundary-value problems (BVP, the describing partial differential equation in combination with the boundary conditions of the analyzed model), which do not match the real objects sufficiently.

This was the reason that we started to investigate bending beam vibrations of technical vibrissae exhibiting a support compliance. First models were analyzed in [16] and presented in [1]. Focussing on our tenor and in order to do the investigations in an analytical way, we neglect the conical shape with respect to the complex structure of the arising partial differential equation. We focus on cylindrical beams.

First models with various elastic supports are presented in Figures 3 and 4.

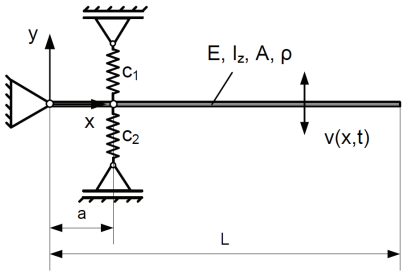

Figure 3. Pivoted vibrissa beam model with modeled skin support (one level of elasticity), [16].

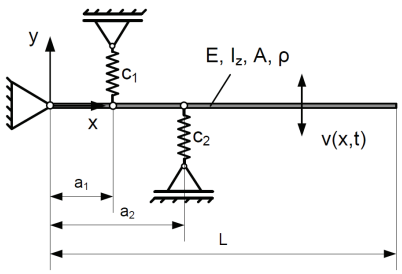

Figure 4. Pivoted vibrissa beam model with two levels of elasticity (FSC and skin), [16].

These models present a cylindrical pivoted beam with various elastics couplings (modeling the compliance of the FSC and skin). The arising BVP could be treated analytically in parts. But, the 'pivot' is at the base, this does not match reality.

Therefore, consider the model in Figure 5. The pivot is shifted, but the system is still undamped. Finally, we developed the model given in Figure 6.

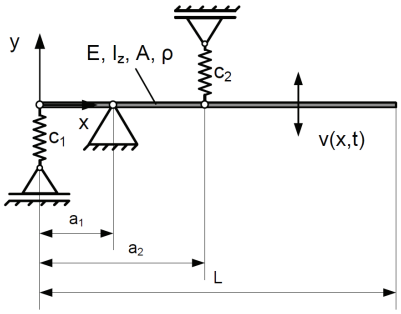

Figure 5. Undamped vibrissa beam model with modeled skin and FSC support, [16].

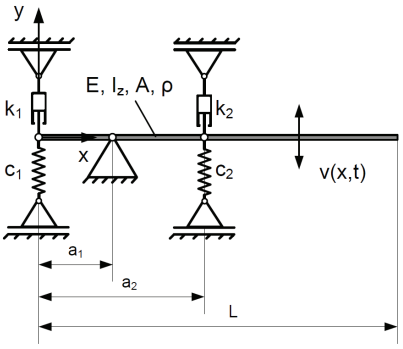

Figure 6. Damped vibrissa beam model with modeled skin and FSC support, [16].

In [1], we summarized for these models

- ⊖ Neglecting the conical shape of the vibrissa
- ⊕ Consideration of the support's compliance
  - · at skin level
  - · at the level of the FSC
- ⊕ Finding: massive influence of the support on the natural frequencies
- ⊕ Finding: influence of damping elements in the support
  - ↪ massive for the 1^{st} natural frequency
  - ↪ but: unlike behavior of the natural frequencies (increasing frequencies if the system is damped, this contradicts the classical assertions)

IV. Goal and Arrangement of the Following Work

As mentioned above, we try to make the vibrissa models more realistic to the biological paradigm, but not too complex as the models in Figures 3 to 6. We present various approaches to implement and to determine the basic features of animal vibrissae as mentioned in Section II. Here, we will focus on the mechanical properties and the dynamic behavior of the vibrissa beam models. The processing of the stimulus and the corresponding analysis of different control strategies are **not** discussed here. Furthermore, the investigations are addressed to a single vibrissa – the interaction between the different vibrissae in the mystacial pad is **not** taken into account. We just want to investigate the unlike behavior of the natural frequencies of these technical vibrissa as pointed out above.

To do this, we start with the classical differential equation for small bending vibrations of beams (linear Euler-Bernoulli theory) in the next Section V. We end up that section with an illustrating example in deriving the frequency spectrum.

Then, we set up and analyze various vibrissa beam models with different supports using discrete and continuously distributed spring and damping elements to mimic tissues of FSC and skin in Sections VI, VII and VIII. Following [24], we focus on the determination of the natural frequency spectrum of such beams analytically and numerically, while varying the viscoelastic properties of the support to check if some unlike behavior of the spectrum occurs. We will **not** focus on static bending problems in the following.

V. Introduction to Transversal Vibrations of Beams

The classical differential equation for small bending vibrations of beams (linear Euler-Bernoulli theory) is the basis of the investigations. Let us start with the following example: a one-sided clamped beam with elastic support (spring stiffness c) at the end, see Figure 7. The beam has length L, Young's modulus E, density ϱ, constant cross section area A and second moment of area I_z. We are seeking for the first five *natural frequencies.*

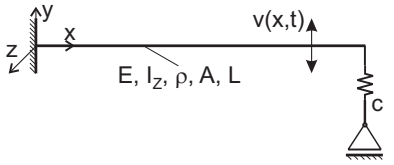

Figure 7. One-sided clamped beam with elastic end support.

Remark V.1. *We focus on the first five natural frequencies of the spectrum because of*

1. *mathematical reasons: the first three to five natural frequencies will form a good approximation basis of the Fourier series of the solution made by the method of separation of variables; and*
2. *physical meanings – higher natural frequencies are too large, whereas only lower ones are perceptible by means of tactile sense.*

The well-known equation of motion for free vibrations of a beam with small deformations, as in Figure 7, is [11]:

$$\ddot{v}(x,t) + k^4\, v''''(x,t) = 0\,, \quad \text{with} \quad k^4 := \frac{E\, I_z}{\varrho\, A}\,, \qquad (1)$$

where the function $v(x,t)$ describes the vertical displacement at point x and at time t.

The partial differential equation (PDE) (1) and the following boundary conditions

①: $v(0,t) = 0 \; \forall\, t \geq 0$
②: $v'(0,t) = 0 \; \forall\, t \geq 0$
③: $v''(L,t) = 0 \; \forall\, t \geq 0$
④: $v'''(L,t)\, E\, I_z - c\, v(L,t) = 0 \; \forall\, t \geq 0$
form a BVP.

Now, we apply the *method of separation of variables*, i.e., we are seeking for special solutions of structure

$$v(x,t) = X(x) \cdot T(t) \quad \forall\, (x,t)\,. \tag{2}$$

Substitution into (1) yields two ordinary differential equations (ODEs)

$$\frac{\ddot{T}(t)}{T(t)} = -\mu^2\,, \tag{3}$$

$$-k^4\, \frac{X''''(x)}{X(x)} = -\mu^2\,. \tag{4}$$

The general solution of (3) is

$$T(t) = \underline{B}_1\, e^{i\,\mu\,t} + \underline{B}_2\, e^{-i\,\mu\,t}\,,\; \underline{B}_1, \underline{B}_2 \in \mathbb{C}\,. \tag{5}$$

The solution of (4) is:

$$\begin{aligned} X(x) = C_1\, \cos(\lambda\, x) + C_2\, \sin(\lambda\, x) \\ + C_3\, \cosh(\lambda\, x) + C_4\, \sinh(\lambda\, x)\,. \end{aligned} \tag{6}$$

with $C_1, C_2, C_3, C_4 \in \mathbb{C}$ and

$$\boxed{\lambda^4 := \tfrac{\mu^2}{k^4}\,, \qquad k^4 := \tfrac{E\, I_z}{\varrho\, A}\,.} \tag{7}$$

This shape solution (6) together with the formulated four boundary conditions form an eigenvalue problem (EVP) in the following. We get $\forall\, t \geq 0$

$$\begin{aligned}
&① \quad T(t)\; (C_1 + C_3) = 0 \\
&② \quad T(t)\, \lambda\; (C_2 + C_4) = 0 \\
&③ \quad T(t)\, \lambda^2 \big(- C_1\, \cos(\lambda\, L) - C_2\, \sin(\lambda\, L) \\
&\qquad\qquad + C_3\, \cosh(\lambda\, L) + C_4\, \sinh(\lambda\, L)\big) = 0 \\
&④ \quad E\, I_z\, T(t)\, \lambda^3 \big(C_1\, \sin(\lambda\, L) - C_2\, \cos(\lambda\, L) \\
&\quad + C_3\, \sinh(\lambda\, L) + C_4\, \cosh(\lambda\, L)\big) \\
&\qquad - c\, T(t)\, \big(C_1\, \cos(\lambda\, L) + C_2\, \sin(\lambda\, L) \\
&\qquad\qquad + C_3\, \cosh(\lambda\, L) + C_4\, \sinh(\lambda\, L)\big) = 0
\end{aligned}$$

$T(t)$ drops and a system of homogenous linear equations results with a coefficient matrix (8).

Since we are seeking for non-trivial solutions, we claim the singularity of the coefficient matrix: $\det(M) = 0$. Introducing a ratio of elasticity

$$\gamma_c := \frac{c}{c_S} = \frac{c}{\frac{E\, I_z}{L^3}} = \frac{c\, L^3}{E\, I_z}$$

we obtain the characteristic eigenvalue equation

$$\begin{aligned} &\lambda^3\, L^3\; (1 + \cosh(\lambda\, L)\, \cos(\lambda\, L)) \\ &+ \gamma_c\; (\cosh(\lambda\, L)\, \sin(\lambda\, L) - \cos(\lambda\, L)\, \sinh(\lambda\, L)) = 0 \end{aligned} \tag{9}$$

Remark V.2. *Before solving* (9) *we check it in setting*

- $c = 0$*: we get* $1 + \cosh(\lambda\, L)\, \cos(\lambda\, L) = 0$*, which forms the eigenvalue equation of an one-sided clamped / free end beam in Figure 8;*
- $c \to +\infty$*: we get* $\cosh(\lambda\, L)\, \sin(\lambda\, L) - \cos(\lambda\, L)\, \sinh(\lambda\, L) = 0$*, which arises for a clamped beam with bearing in Figure 9.*

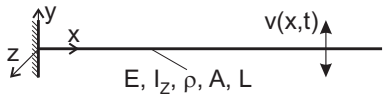

Figure 8. One-sided clamped beam with free end.

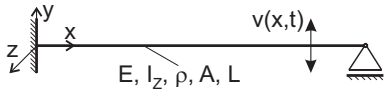

Figure 9. One-sided clamped beam with bearing.

Now, we present some numerical calculations. We choose $\gamma_c = 1$ and derive the natural frequencies of a steel beam and of a $B2$ vibrissa, see Figure 1, using the following parameters:

- steel beam: $E = 210\,\text{GPa}$, $\varrho = 7850\,\frac{\text{kg}}{\text{m}^3}$;
- $B2$ vibrissa: $E = 2.3\,\text{GPa}$, $\varrho = 238.732\,\frac{\text{kg}}{\text{m}^3}$;
- geometric parameters: $d = 0.2\,\text{mm}$, $I_z = \frac{\pi}{64}\, d^4$, $A = \frac{\pi}{4}\, d^2$, $L = 40\,\text{mm}$.

The following Table I presents the first five eigenvalues λ_j, natural frequencies ω_j in rad/s and frequencies f_j in Hz for a steel beam and a $B2$ vibrissa.

TABLE I. Calculation for $\gamma_c = 1$.

		steel beam		$B2$ vibrissa	
j	λ_j	ω_j	f_j	ω_j	f_j
1	$2.010\,\frac{1}{L}$	653.008	103.929	843.189	62.369
2	$4.704\,\frac{1}{L}$	3576.197	569.169	4617.724	341.566
3	$7.857\,\frac{1}{L}$	9977.433	1587.958	12883.248	952.955
4	$10.996\,\frac{1}{L}$	19544.181	3110.553	25236.203	1866.685
5	$14.138\,\frac{1}{L}$	32305.127	5141.521	41713.630	3085.496

Increasing γ_c leads to increasing ω_j, see also [1]. In the following, we increase the level of complexity.

VI. Vibrissa Model 1: Translational Viscoelasticity

To clarify the unlike effects of the foregoing subsection, we deal with a 'simple' problem to investigate the influence of discrete damping elements. We consider a cylindrical, one-sided clamped beam, which is viscoelastically supported at the end, see Figure 10, which forms a subsystem of the complex one presented in Figure 6.

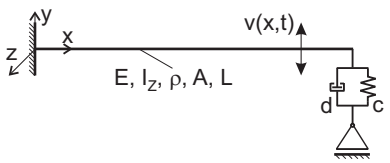

Figure 10. Clamped beam with viscoelastic end support.

$$M(\lambda) := \begin{pmatrix} 1 & \vdots & 0 & \vdots & 1 & \vdots & 0 \\ \cdots & \cdots & \cdots & \cdots & \cdots & \cdots & \cdots \\ 0 & \vdots & \lambda & \vdots & 0 & \vdots & \lambda \\ \cdots & \cdots & \cdots & \cdots & \cdots & \cdots & \cdots \\ \cos(\lambda L)\,\lambda^2 & \vdots & \sin(\lambda L)\,\lambda^2 & \vdots & \cosh(\lambda L)\,\lambda^2 & \vdots & \sinh(\lambda L)\,\lambda^2 \\ \cdots & \cdots & \cdots & \cdots & \cdots & \cdots & \cdots \\ E\,I_z\,\sin(\lambda L)\,\lambda^3 & \vdots & -E\,I_z\,\cos(\lambda L)\,\lambda^3 & \vdots & E\,I_z\,\sinh(\lambda L)\,\lambda^3 & \vdots & E\,I_z\,\cosh(\lambda L)\,\lambda^3 \\ -c\,\cos(\lambda L) & \vdots & -c\,\sin(\lambda L) & \vdots & -c\,\cosh(\lambda L) & \vdots & -c\,\sinh(\lambda L) \end{pmatrix} \tag{8}$$

Equation (1) together with the boundary conditions

$$\begin{aligned} v(0,t) &\equiv 0 \\ v'(0,t) &\equiv 0 \\ v''(L,t) &\equiv 0 \\ E\,I_z\,v'''(L,t) - d\,\dot{v}(L,t) - c\,v(L,t) &\equiv 0\,, \end{aligned}$$

forms a BVP.

The handling of the last boundary condition results in

$$E\,I_z\,X'''(L) - c\,X(L) = \pm\,i\,d\,\lambda^2\,k^2\,X(L)\,.$$

All conditions lead to a coefficient matrix (not listed here for brevity) of the homogenous systems whose singularity yields the eigenvalue equation (EVEQ):

$$\begin{aligned} \det\left(A(\lambda)\right) = &-E\,I_z\,\lambda^3 \\ &- E\,I_z\,\cos\left(\lambda\,L\right)\,\cosh\left(\lambda\,L\right)\,\lambda^3 \\ &\pm\,i\,d\,k^2\,\sin\left(\lambda\,L\right)\,\cosh\left(\lambda\,L\right)\,\lambda^2 \\ &- c\,\sin\left(\lambda\,L\right)\,\cosh\left(\lambda\,L\right) \\ &\mp\,i\,d\,k^2\,\cos\left(\lambda\,L\right)\,\sinh\left(\lambda\,L\right)\,\lambda^2 \\ &+ c\,\cos\left(\lambda\,L\right)\,\sinh\left(\lambda\,L\right) = 0\,. \end{aligned} \tag{10}$$

Remark VI.1. *At this stage, we could check this equation in concluding well-known eigenvalue equations: setting $\{d = 0, c = 0\}$ we get the EVEQ of system in Figure 8, or $\{d = 0, c > 0\}$ of model in Figure 7, or $\{d = 0, c \to +\infty\}$ of model in Figure 9, all results in the equations presented in [11] or [28].*

Introducing the dimensionless parameters

$$\begin{aligned} c^* &:= \frac{c}{\frac{E I_z}{L^3}} \\ d^* &:= \frac{L\,d}{\sqrt{\varrho\,A\,E\,I_z}}\,, \end{aligned}$$

we determine the first three natural frequencies in varying c^* and d^*. (From now, we drop the notation '$*$' as a mark for a dimensionless parameter for brevity.) We get the following Figures 11 to 13.

For fixed c and varying d, there are parameter ranges of c where we get an expected and unexpected behavior of the first natural frequency, see Figure 11:

- $c \in [0, 17]$: the natural frequency breaks down to zero for increasing d;
- $c \in [18, 23]$: first, the natural frequency increases and then breaks down to zero;

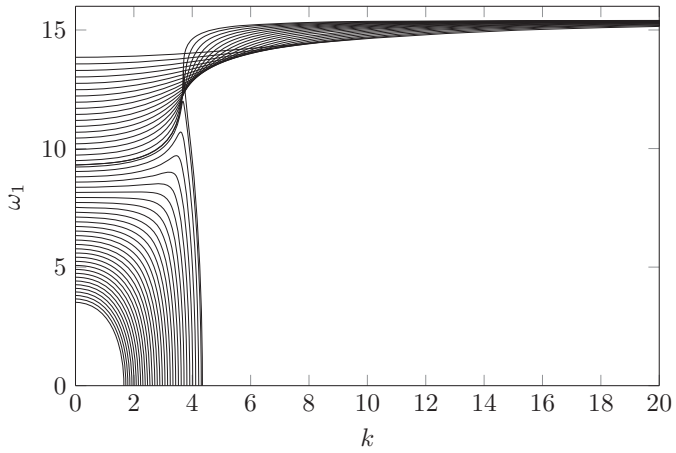

Figure 11. First natural frequency of the beam model ω_1 in $\sqrt{\frac{E\,I_z}{\varrho\,A\,L^4}}$ in dependence on c and d.

- $c > 23$: the natural frequency just increases.

On the other hand, for fixed d and varying c, we observe the following:

- $d \in [0, 3.5]$: increasing c leads to an increase of the natural frequency;
- $d > 3.5$: an increase of c results first in a decrease and then in an increase of the natural frequency.

This may explain the behaviors of the natural frequencies described above and presented in [1], which contradicts the classical assertions.

Similar effects can be observed in Figures 12 and 13.

VII. Vibrissa Model 2: Rotational Viscoelasticity

Since the vibrissa system in Figure 10 forms not really a bio-inspired vibrissa system, we soften the clamping to a bearing with a torsional spring and damper element, see Figure 14.

The boundary condition have changed to

$$\begin{aligned} v(0,t) &\equiv 0 \\ E\,I_z\,v''(0,t) - c_t\,v'(0,t) - d_t\,\dot{v}'(0,t) &\equiv 0 \\ v''(L,t) &\equiv 0 \\ v'''(L,t) &\equiv 0\,. \end{aligned}$$

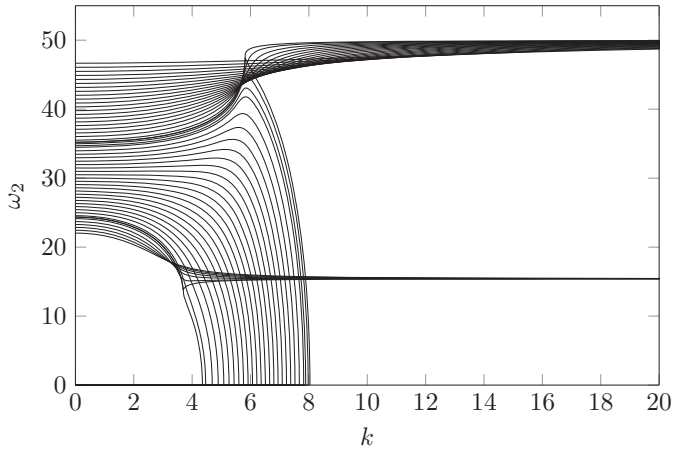

Figure 12. Second natural frequency of the beam model ω_2 in $\sqrt{\frac{E\,I_z}{\varrho\,A\,L^4}}$ in dependence on c and d.

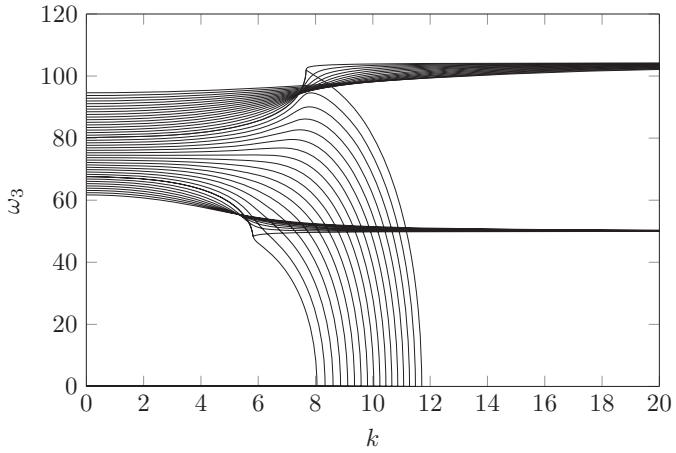

Figure 13. Third natural frequency of the beam model ω_3 in $\sqrt{\frac{E\,I_z}{\varrho\,A\,L^4}}$ in dependence on c and d.

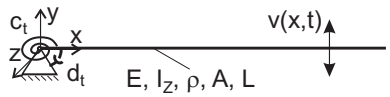

Figure 14. Vibrissa model with a bearing and torsional spring-damper element.

Introducing the dimensionless parameters

$$c_t{}^* := \frac{c_t}{\frac{E I_z}{L}}$$

$$d_t{}^* := \frac{d_t}{L\sqrt{\varrho\,A\,E\,I_z}}\,,$$

we determine the first three natural frequencies in varying $c_t{}^*$ and $d_t{}^*$. (Once again, we omit the notation '$*$' for brevity.) We get the following EVEQ:

$$\lambda\,(\cos(\lambda)\,\sinh(\lambda)\sin(\lambda)\,\cosh(\lambda)) \\ (\cos(\lambda)\,\cosh(\lambda)+1)\,\left(c_t \pm i\,\lambda^2\,d_t\right) = 0\,. \quad (11)$$

Solving this EVEQ in λ and determination of the corresponding natural frequencies we get the natural frequency behavior presented in Figures 15 to 17.

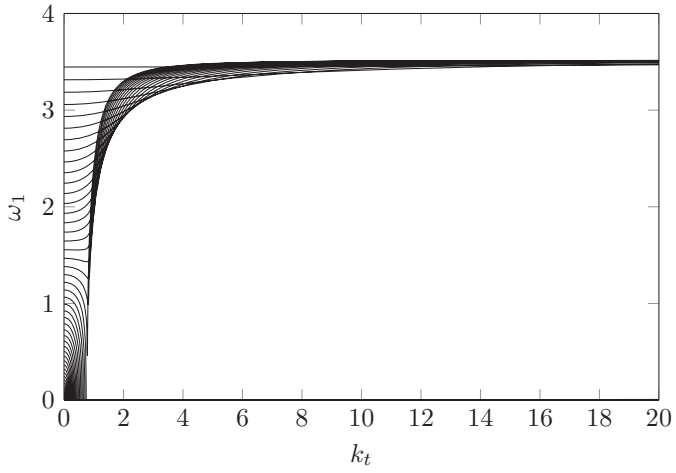

Figure 15. First natural frequency of the beam model ω_1 in $\sqrt{\frac{E\,I_z}{\varrho\,A\,L^4}}$ in dependence on c_t and d_t.

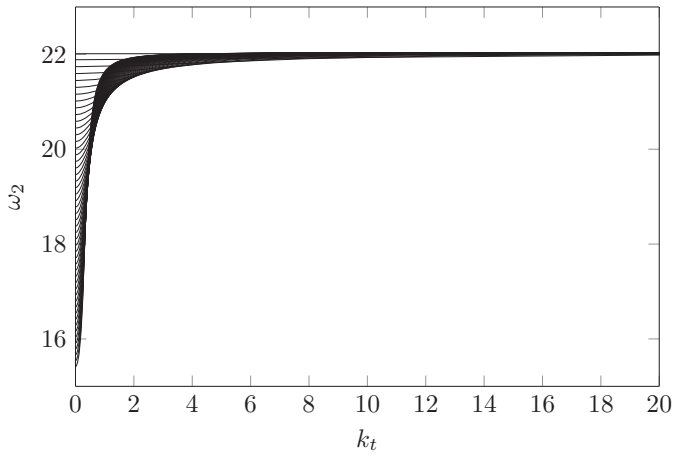

Figure 16. Second natural frequency of the beam model ω_1 in $\sqrt{\frac{E\,I_z}{\varrho\,A\,L^4}}$ in dependence on c_t and d_t.

One can clearly see that only the first natural frequency exhibit a similar unlike behavior, because some curves break down to zero. If c_t has a special value, then if c_t and / or d_t increases to infinity, the natural frequency ω_1 tends to the first natural frequency of system in Figure 8. This behavior can be seen in observing ω_2 in Figure 16 and ω_3 in Figure 17 from the very beginning, which is a typical behavior of natural frequencies.

VIII. Vibrissa Model 3: Translational and Rotational Viscoelasticity

Now, we use the model of Section VII and combine it with an additional support mimicking a sudden obstacle contact modeled as a translational viscoelastic support, see Figure 18.

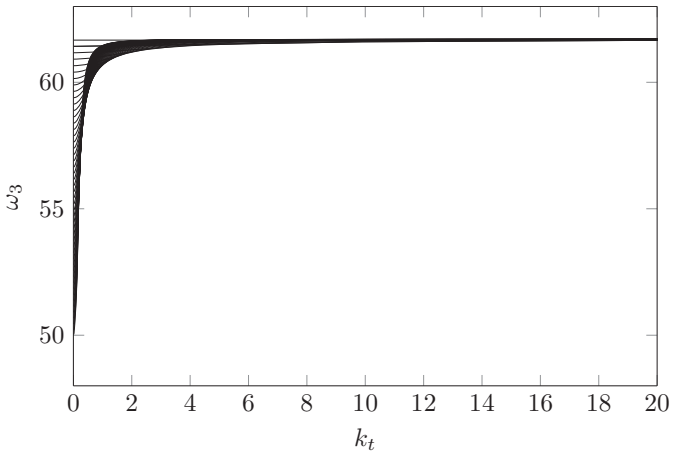

Figure 17. Third natural frequency of the beam model ω_1 in $\sqrt{\frac{E\,I_z}{\varrho\,A\,L^4}}$ in dependence on c_t and d_t.

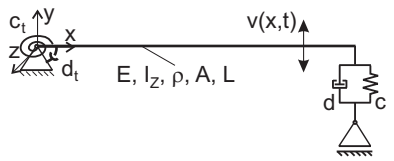

Figure 18. Vibrissa model with object contact: torsional spring-damper-bearing and viscoelastic end support.

We suppose that the vibrissa contacts the object with the tip, as in [8] and [9], such that model consideration is valid. Now, the upcoming calculation shall later provide the determination of the shift of the spectrum of natural frequencies to determine the distance to the object. For this, we need to have a reliable determination of the spectrum, still exhibiting unlike effects described above.

The boundary condition are now

$$\begin{aligned} v(0,t) &\equiv 0 \\ E\,I_z\,v''(0,t) - c_t\,v'(0,t) - d_t\,\dot{v}'(0,t) &\equiv 0 \\ v''(L,t) &\equiv 0 \\ E\,I_z\,v'''(L,t) - d\,\dot{v}(L,t) - c\,v(L,t) &\equiv 0\,. \end{aligned}$$

Performing the same procedure in deriving the EVEQ as above, we get

$$\begin{aligned} \lambda^3\Big\{\lambda\,(\cosh(\lambda)\,\sin(\lambda) - \sinh(\lambda)\,\cos(\lambda)) \\ - \left(c_t \pm i\,d_t\,\lambda^2\right)\,(1 + \cosh(\lambda)\,\cos(\lambda))\Big\} \\ - \left(c \pm i\,d\,\lambda^2\right)\Big\{\lambda\,\sinh(\lambda)\,\sin(\lambda) \\ + \left(c_t \pm i\,d_t\,\lambda^2\right)\,(\cosh(\lambda)\,\sin(\lambda) - \sinh(\lambda)\,\cos(\lambda))\Big\} = 0\,. \end{aligned} \tag{12}$$

Several investigations / scenarios are conceivable. We only focus on the following two cases:

- Case 1: a parameter dependence of the natural frequencies on the 'FSC' support parameters c_t and d_t is performed, where we choose $c = 1$ and $k = 1$ fix.
- Case 2: a dependence of the natural frequencies on the 'contact' parameters c and d is analyzed, where we choose $c_t = 100$ and $d_t = 20$.

In Case 1, we get describe a soft object contact with the chosen parameters. Hence, we have the possibility to do comparison to Section VII. One can clearly see the similarity of Figures 15 to 17 with Figures 19 to 21.

Here are more parameter studies necessary to get more familiar with this system. If we use such a system in later experiments, we could be able to detect not only the distance to an object (as done in [9]) but also the compliance of the object.

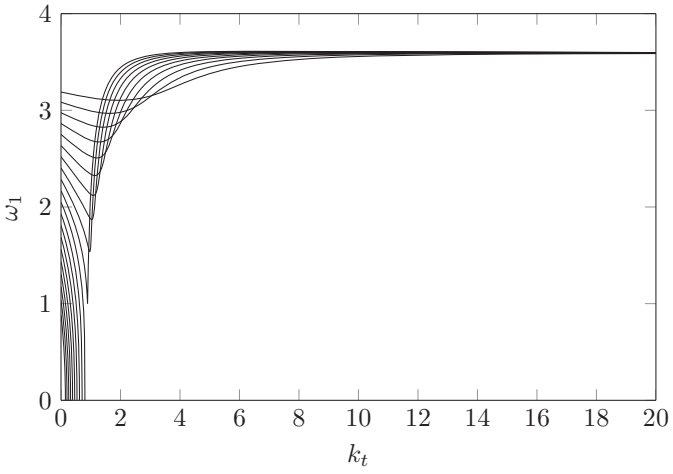

Figure 19. First natural frequency of the beam model ω_1 in $\sqrt{\frac{E\,I_z}{\varrho\,A\,L^4}}$ in dependence on c_t and d_t.

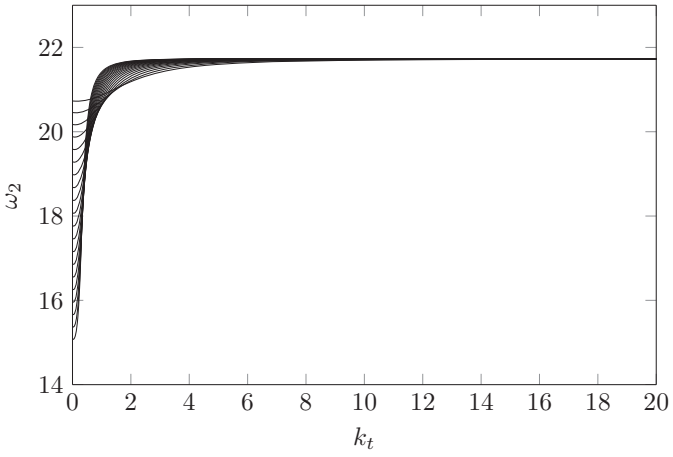

Figure 20. Second natural frequency of the beam model ω_1 in $\sqrt{\frac{E\,I_z}{\varrho\,A\,L^4}}$ in dependence on c_t and d_t.

In Case 1, we get describe a soft object contact with the chosen parameters. Hence, we have the possibility to do comparison to Section VII. One can clearly see the similarity of Figures 15 to 17 with Figures 19 to 21.

Here are more parameter studies necessary to get more familiar with this system. If we use such a system in later

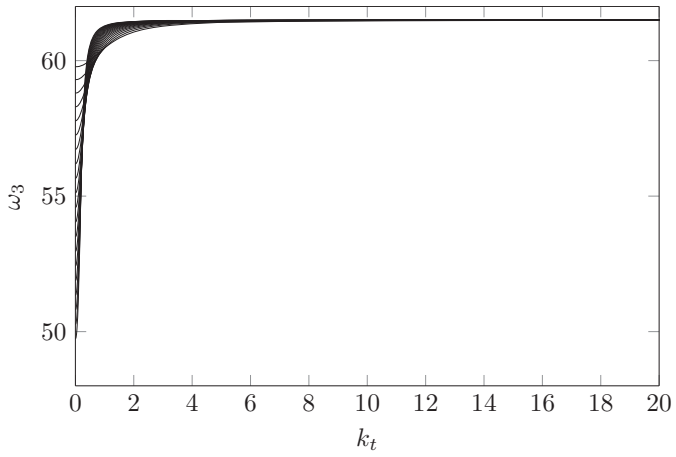

Figure 21. Third natural frequency of the beam model ω_1 in $\sqrt{\frac{E\,I_z}{\varrho\,A\,L^4}}$ in dependence on c_t and d_t.

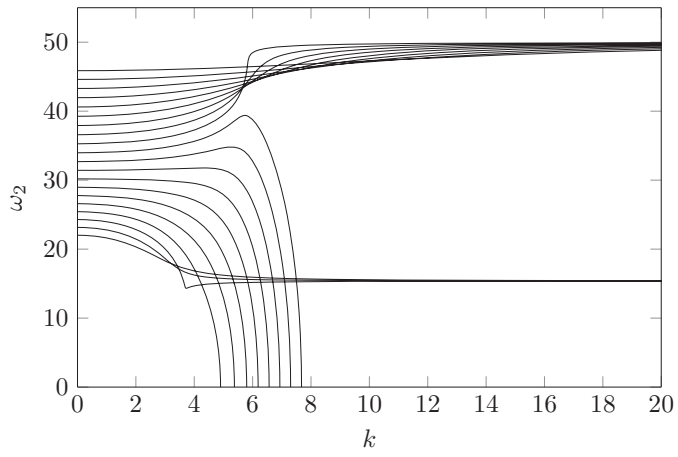

Figure 23. Second natural frequency of the beam model ω_1 in $\sqrt{\frac{E\,I_z}{\varrho\,A\,L^4}}$ in dependence on c_t and d_t.

experiments, we could be able to detect not only the distance to an object (as done in [9]) but also the compliance of the object.

In Case 2, we focus on a 'hard' bearing (or nearly a clamping), so that comparison to Section VI can be done. We have a similar behavior of the natural frequencies if someone inspects Figures 11 to 13 with Figures 22 to 24.

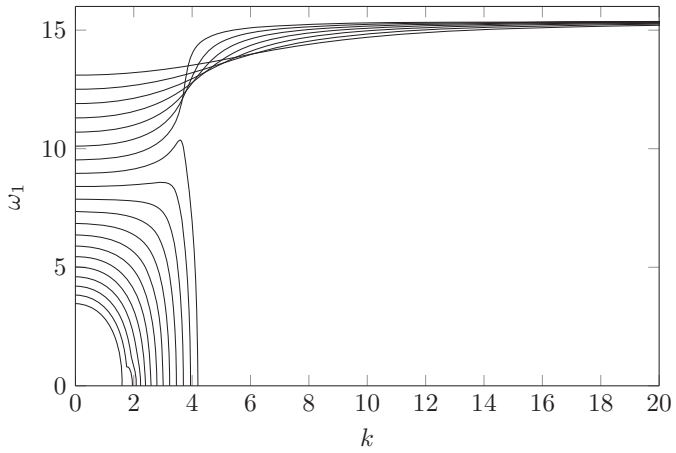

Figure 22. First natural frequency of the beam model ω_1 in $\sqrt{\frac{E\,I_z}{\varrho\,A\,L^4}}$ in dependence on c_t and d_t.

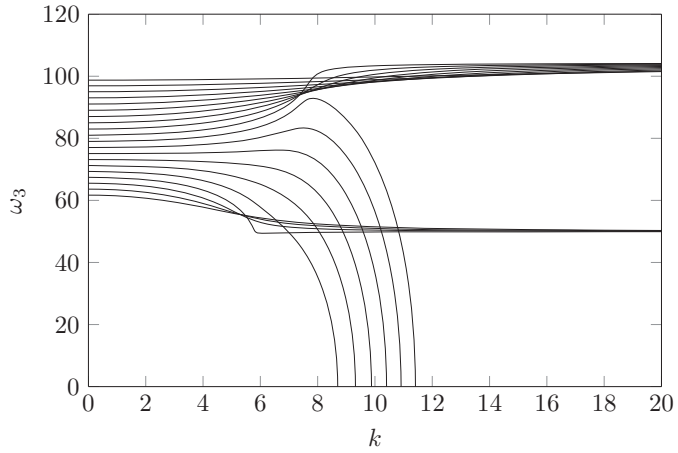

Figure 24. Third natural frequency of the beam model ω_1 in $\sqrt{\frac{E\,I_z}{\varrho\,A\,L^4}}$ in dependence on c_t and d_t.

Summarizing, the unlike behavior appears also in combined systems and is not a numerical feature. More investigation should be done, before coming to real prototypes of artificial vibrissa-like sensors.

IX. Conclusion

The goal of this contribution was to present the theoretical context needed to examine the mechanical and in particular the dynamical characteristics of the biological vibrissa. Moreover, these theoretical aspects were to be interpreted with respect to the biological vibrissa, as well as for a technical implementation of it. Inspired by this biological sensory system, several types of mechanical models were developed based on findings in the literature.

The second focus was on the modeling of the vibrissa as a *continuous system*: bending vibrations of beams. There, the main focus of the studies lay on the examination of the influence of the tactile hair compliance and the viscoelastic support on the oscillation characteristics of the vibrissa. The conical form was neglected until now.

The influence of the viscoelastic support of the vibrissa has been examined using various abstract models, in which the vibrissa was modeled as a thin, cylindrical, flexible beam. The viscoelastic properties of the FSC and the skin were implemented by using spring and damping elements.

The damping element significantly increased the complexity of the differential equations and led to a surprising phenomenon: there exist some natural frequencies, which break down to zero for a certain range of parameters. This fact is well-known in 1-DoF systems (i.e., strong damping, creeping behavior). The study demonstrated that the oscillation behavior of an elastic beam differs remarkably from the behavior of such

a classical system:

- The natural frequencies may increase with growing boundary damping.
- For specific damping parameter values, the natural frequencies grow for decreasing boundary stiffness.

This behavior also occurred in other developed vibrissa-like sensor systems, which are much closer to the real paradigm, also in context of an object contact.

But, theories gained from the simplified linear Euler-Bernoulli theory are only valid for small deflections and deformations. If one considers a vibrissa beam in passive mode, then it may be questionable if this theory is really qualified for the investigations, see large bending deformations. Inspecting these vibrissa configurations, one could clearly observe that the vibrissa in passive mode suffers large deformations. Hence, the linear Euler-Bernoulli theory is not qualified to determine the natural frequencies since it describes the bending behavior for small deformations. We have to turn to a nonlinear theory – Timoshenko theory or nonlinear Euler-Bernoulli theory. We will arrive at more realistic models and description of these models, which then are closer to the biological paradigm. An approach is done in [29].

However, we are focussing on long, slender beams, whereby shear forces may have less influence. So, we shall focus on the nonlinear Euler-Bernoulli theory in future work. Additionally, we shall include the conical shape and a pre-curvature of the beam, neglected until now.

The first works, setting up a prototype of these investigations, can be found in [9] and [27].

REFERENCES

[1] C. Behn, C. Will, and J. Steigenberger, "Unlike Behavior of Natural Frequencies in Bending Beam Vibrations with Boundary Damping in Context of Bio-inspired Sensors," in *Proceedings INTELLI 2014: The Third International Conference on Intelligent Systems and Applications,* Sevilla (Spain), June 2014, IARIA, pp. 75–84.

[2] A. Birdwell et al., "Biomechanical Models for Radial Distance Determination by the Rat Vibrissal System," *The Journal of Neurophysiology,* vol. 98, pp. 2439–2455, 2007.

[3] D. Kim and R. Möller, "Biomimetic whiskers for shape recognition," *Robotics and Autonomous Systems,* vol. 55, no. 3, pp. 229-243, 2007.

[4] C. Tuna, J. H. Solomon, D. L. Jones, and M. J. Hartmann, "Object shape recognition with artificial whiskers using tomographic reconstruction," in *IEEE International Conference on Acoustics, Speech and Signal Processing (ICASSP),* pp. 2537-2540, 2012.

[5] C. Will, J. Steigenberger, and C. Behn, "Object Contour Reconstruction using Bio-inspired Sensors," in *Proceedings 11th International Conference on Informatics in Control, Automation and Robotics (ICINCO 2014),* Vienna (Austria), September 2014, SciTePress, pp. 459–467, 2014.

[6] C. Will, J. Steigenberger, and C. Behn, "Quasi-static object scanning using technical vibrissae," in *Proceedings 58th International Scientific Colloquium,* Ilmenau (Germany), September 2014.

[7] S. Hirose, S. Inoue, and K. Yoneda, "The whisker sensor and the transmission of multiple sensor signals," *Advanced Robotics,* vol. 4, no. 2, pp 105-117, 1989.

[8] N. Ueno, M. M. Svinin, and M. Kaneko, "Dynamic contact sensing by flexible beam," *IEEE/ASME Trans. Mechatronics,* vol. 3, no. 4, pp. 254–264, 1998.

[9] D. Baldeweg, C. Will, and C. Behn, "Tranversal Vibrations of Beams in Context of Vibrissae with Foundations, Discrete Supports and Various Sections," in *Proceedings 58th International Scientific Colloquium,* Ilmenau (Germany), September 2014.

[10] H. Pierson, J. Brevick, and K. Hubbard, "The effect of discrete viscous damping on the transverse vibration of beams," *Journal of Sound and Vibration,* vol. 332, pp. 4045–4053, 2013.

[11] W. Weaver, S. P. Timoshenko, and D. H. Young, *Vibration Problems in Engineering.* John Wiley & Sons Inc., Chichester, 1990.

[12] D. Voges et al., "Structural characterisation of the whisker system of the rat," *IEEE Sensors Journal,* vol. 12, no. 2, pp. 332–339, 2012.

[13] J. Dörfl, "The musculature of the mystacial vibrissae of the white mouse," *Journal of Anatomy,* vol. 135, pp. 147–154, 1982.

[14] T.-E. Jin, V. Witzemann, and M. Brecht, "Fiber Types of the Intrinsic Whisker Muscle and Whisking Behavior," *The Journal of Neuroscience,* vol. 24, no. 13, pp. 3386–3393, 2004.

[15] D. R. Soderquist, *Sensory processes.* Sage Publications, Thousand Oaks, 2002.

[16] C. Behn, "Mathematical Modeling and Control of Biologically Inspired Uncertain Motion Systems with Adaptive Features," Habilitation thesis, Faculty of Mechanical Engineering, Ilmenau University of Ilmenau, Germany, 2013.

[17] C. Behn, "Modeling the Adjustment of Receptor Cells via Adaptive λ-Stabilizing-Control," *Journal of Mechatronics,* vol. 2, no. 4, pp. 275–290, 2014.

[18] C. Behn, "Modeling, Analysis and Control of Mechanoreceptors with Adaptive Features," in *Infomatics in Control, Automation and Robotics — Lecture Notesd in Electrical Engineering (LNEE),* vol. 325, J.-L. Ferrier et al. (eds.), Springer International Publishing, Switzerland, pp. 349–366, 2015.

[19] J. Dörfl, "The innervation of the mystacial region of the white mouse – A topographical study," *Journal of Anatomy,* vol. 142, pp. 173–184, 1985.

[20] L. E. Wineski, "Facial morphology and vibrissal movement in the golden hamster," *Journal of Morphology,* vol. 183, pp. 199–217, 1985.

[21] S. Haidarliu, E. Simony, D. Golomb, and E. Ahissar, "Muscle Architecture in the Mystacial Pad of the Rat," *The Anatomical Record,* vol. 293, pp. 1192–1206, 2010.

[22] M. J. Hartmann and J. H. Solomon, "Robotic whiskers used to sense features: Whiskers mimicking those of seals or rats might be useful for underwater tracking or tactile exploration," *NATURE,* vol. 443, p. 525, 2006.

[23] K. Carl, *Technische Biologie des Tasthaar-Sinnessystems als Gestaltungsgrundlage für taktile stiftführende Mechanosensoren, Technical biology of the vibrissa sensor system as design principles for tactile mechanosensors.* PhD thesis, Universitätsverlag, Ilmenau, 2009.

[24] M. A. Neimark, M. L. Andermann, J. J. Hopfield, and C. I. Moore, "Vibrissa Resonance as a Transduction Mechanism for Tactile Encoding," *The Journal of Neuroscience,* vol. 23, no. 16, pp. 6499–6509, 2003.

[25] M. L. Andermann, J. Ritt, M. Neimark, and C. I. Moore, "Neural Correlates of Vibrissa Resonance: Band-Pass and Somatotopic Representation of High-Frequency Stimuli," *Neuron,* vol. 42, pp. 451–463, 2004.

[26] G. Scholz and C. Rahn, "Profile Sensing With an Actuated Whisker," *IEEE Transactions on Robotics and Automation,* vol. 20, pp. 124–127, 2004.

[27] C. Will, J. Steigenberger, and C. Behn, "Bio-inspired Technical Vibrissae for Quasi-static Profile Scanning," accepted for *Informatics in Control, Automation and Robotics Lecture Notes in Electrical Engineering (LNEE),* Springer, 2016.

[28] D. Gross, W. Hauger, W. Schnell, and P. Wriggers, *Technische Mechanik: Band 4 Hydromechanik, Elemente der Höheren Mechanik, Numerische Methoden, Technical Mechanics: Volume 4 Hydromechanics, higher mechanics, numerical methods.* Springer, Berlin, 2002.

[29] J. H. Solomon and M. J. Hartmann, "Extracting object contours with the sweep of a robotic whisker using torque information," *The International Journal of Robotics Research,* vol. 29, pp. 1233–1245, 2010.